DESIGN TAILORING FOR PRESSURE PILLOWING USING TOW-PLACED STEERED FIBERS

Ahmad Alhajahmad*, Mostafa M. Abdalla*, Zafer Gürdal*
*Delft University of Technology, The Netherlands

Keywords: *steered fibers, variable-stiffness, pressure pillowing, structural optimization*

Abstract

Manufacturing of high quality fiber-reinforced composite structures with spatially varying fiber orientation is possible using advanced tow-placement machines. Changing the fiber orientation angle within a layer produces variable-stiffness properties. Contrary to traditional composites with straight fibers, this method allows the designer to fully benefit from the directional material properties of the composite to improve laminate performance by determining optimal fiber paths.

In this paper, design tailoring for pressure pillowing problem of a fuselage skin is addressed using steered fibers. The problem is modelled as a two-dimensional plate using von Kármán plate equations. The design objective is to determine the optimal fiber paths over the panel for maximum failure load. Different designs are obtained for different loading cases. The results indicate that by using steered fibers the pressure pillowing problem can be alleviated, and the load carrying capacity of the structure can be improved compared to designs with straight fibers.

1 Introduction

One of the primary advantages of using fiber-reinforced laminated composites in structural design is the ability to change the stiffness and strength of the laminate by designing the laminate stacking sequence in order to improve its performance. This flexibility to design the stacking sequence of the laminate is typically referred to as laminate tailoring. Traditionally, tailoring is achieved by keeping the fiber orientation angle within each layer constant throughout a component resulting in constant-stiffness structure. One method of creating variable-stiffness composite structure is by changing the fiber orientation angle continuously within the lamina. Allowing the fibers to curve within the lamina constitutes an advanced tailoring option to account for non-uniform stress states in a continuous manner. By varying the stiffness properties of composite laminates from one point to another, the design space is expanded as compared to the classical stacking sequence design problem. As a consequence, stiffer and/or lighter structures can be obtained.

An intensive study of rectangular panels with curvilinear fiber paths, termed variable-stiffness panels, was carried out by Gürdal et al. [1]. The curvilinear paths in those studies were generated from a base curve that changes its orientation angle linearly from one end of the panel to the other, while taking into account constraints on the radius of curvature of the fiber paths. Despite the fact that linear fiber orientation variation represents only a limited class of spatially varying orientations, earlier studies showed that significant improvements in the laminate response can be obtained for panels with and without holes under compression and shear loads [2-4]. Investigation of the optimal designs for both constant and variable-stiffness composite plates for minimum compliance was performed by Setoodeh et al. [5]. In these latter studies, the lamination parameters were used as design variables instead of fiber orientation angles, thus reducing the number of design variables. Moreover, the formulation guaranteed that the solution is optimal, benefiting from the fact that the optimization problem is convex. Although the actual stacking sequence was unknown, the results showed that substantial improvements in stiffness can be gained by using variable-stiffness designs. In a follow-up work, the curvilinear fiber paths were generated from the lamination parameter distribution [6].

A challenging problem in the aircraft structures associated with thin-walled stiffened structures is the

so-called pressure pillowing. Pressurized fuselages and fuel tanks are typical examples of structures in which pressure pillowing is observed. In the case of fuselages, the cabin pressure causes a significant pressure differential across the skin. An unstiffened fuselage would carry this internal pressure load as a shell in membrane response, like pressure vessels. However, internal longitudinal and transverse stiffeners (stringers and frames as shown in Fig. 1) are necessary to carry maneuver loads. The presence of these stiffeners prevents the fuselage skin from expanding as a membrane, and the skin bulges, or "pillows", within each panel bay under the action of the internal pressure. When the skin is restrained against out-of-plane expansion at the stiffener locations, a bending boundary layer is formed.

Recently, design tailoring for pressure pillowing using variable-stiffness concept has been investigated by Alhajahmad et al.[7]. The pressure pillowing problem was modelled as a one-dimensional clamped-clamped beam-plate in two loading cases. The first case was a one-dimensional plate subjected to pressure and the second one was a one-dimensional plate under combined pressure and in-plane compressive loads. For both loading cases, the optimal fiber paths along the beam-plate length for minimum weight subject to strength constraints were determined. It was shown, in this latter study, that by using steered fibers the pressure pillowing problem can be alleviated, and lighter laminates can be designed compared to designs with straight fibers.
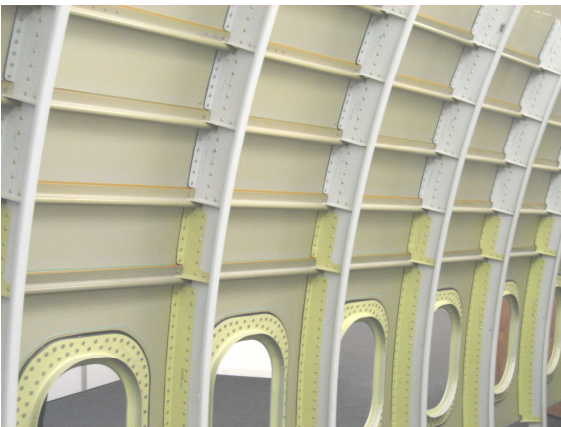
Fig.1. Stiffened structure of a pressurized fuselage (courtesy of Fiber Metal Laminates Center of Competence)

For the analysis of the pressure pillowing problem, the fuselage skin of a panel bay can be modelled using different levels of complexity. Research reported in [7] used a simple beam-plate model, but in general, requires a two-dimensional plate or shallow shell modelling under combined pressure and in-plane loads. Hence, in this paper the problem is modelled as a two-dimensional plate subjected to pressure and in-plane loads. The optimization problem is formulated to determine the optimal fiber paths over the panel for maximum failure load. For optimization purposes, it is of great importance to select an efficient and fast method for the nonlinear analysis. Although the finite element method is a powerful tool for structural analysis problems, the nonlinear nature of the problem at hand makes the use of the finite element undesirable due to excessive computational time required. In this study, the plate problem is approximated using Rayleigh-Ritz method (R-R), and the nonlinear response is traced using normal flow algorithm [8].

2 Problem Formulation

In this paper, a pressurized fuselage skin bounded by two stringers and two frames is modelled as a two-dimensional plate. It is assumed that the skin is flat, balanced and symmetric laminate with a variable-stiffness lay-up $[\pm\theta(x, y)]_{ns}$. The laminate is loaded in two steps. In the first loading step, a uniform pressure p is applied, which is translated into two loads, axial tensile load F_x and hoop tensile load F_y, calculated as

$$F_x = \frac{pR}{2}b\,, \qquad F_y = pRa \qquad (1)$$

where a and b are the length and the width of the plate, respectively, and R is the radius of the fuselage. The pressure and hence the tensile loads are incremented by means of a scaling factor λ_1 in the first loading step. In the second loading step, an additional axial compressive load F_x^B, which results from fuselage bending, is applied. This latter load is incremented by means of a scaling factor λ_2 while keeping λ_1 fixed at the end of the first loading step.

In this work, two loading cases will be investigated, a plate subjected to pressure only (no pressure-induced tensile loads), and a plate subjected to a combination of pressure and in-plane tensile loads applied in the first loading step besides an in-plane compressive load which is applied in the second loading step.

The panel boundary conditions are clamped at ($x = 0$, $x = a$) simulating the panel edges at the frame locations, and simply supported at ($y = 0$, $y = b$) simulating the panel edges at the stringer locations. The fuselage panel model is shown in Fig. 2.
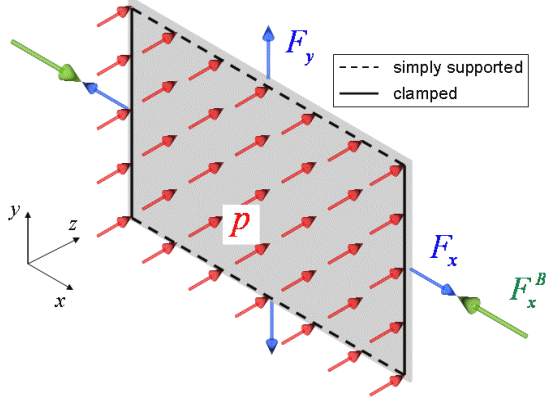
Fig. 2. Fuselage panel model

3 Analysis Formulation

Assuming that the plate is thin, such that the Kirchhoff hypothesis is valid, the laminate strains are expressed in the following form [9]

$$\{\varepsilon\} = \{\varepsilon^0\} + z\{\kappa\} \tag{2}$$

where $\{\varepsilon^0\}$ and $\{\kappa\}$ denote the mid-plane strains and curvatures, respectively. In the moderately large rotation case, according to the von Kármán model, the mid-plane strains and curvatures are given by

$$\{\varepsilon^0\} = \begin{Bmatrix} \varepsilon_x^0 \\ \varepsilon_y^0 \\ \gamma_{xy}^0 \end{Bmatrix} = \begin{Bmatrix} \dfrac{\partial u^0}{\partial x} + \dfrac{1}{2}\left(\dfrac{\partial w}{\partial x}\right)^2 \\ \dfrac{\partial v^0}{\partial y} + \dfrac{1}{2}\left(\dfrac{\partial w}{\partial y}\right)^2 \\ \dfrac{\partial u^0}{\partial y} + \dfrac{\partial v^0}{\partial x} + \dfrac{\partial w}{\partial x}\dfrac{\partial w}{\partial y} \end{Bmatrix} \tag{3}$$

$$\{k\} = \begin{Bmatrix} \kappa_x \\ \kappa_y \\ \kappa_{xy} \end{Bmatrix} = \begin{Bmatrix} -\dfrac{\partial^2 w}{\partial x^2} \\ -\dfrac{\partial^2 w}{\partial y^2} \\ -2\dfrac{\partial^2 w}{\partial x \partial y} \end{Bmatrix} \tag{4}$$

where u^0, v^0, and w are the mid-plane displacements.

Following the Rayleigh-Ritz procedure [10], the total potential energy is given by

$$\Pi = U - W \tag{5}$$

where U is the strain energy, and W is the potential energy of the external loads.

For symmetric and balanced laminates, the strain energy in terms of the mid-plane strains and curvatures is given by

$$U = \frac{1}{2}\int_0^a\int_0^b \begin{bmatrix} A_{11}(\varepsilon_x^0)^2 + A_{22}(\varepsilon_y^0)^2 + \\ 2A_{12}\varepsilon_x^0\varepsilon_y^0 + A_{66}(\gamma_{xy}^0)^2 + \\ D_{11}\kappa_x^2 + D_{22}\kappa_y^2 + 2D_{12}\kappa_x\kappa_y + \\ 2D_{16}\kappa_x\kappa_{xy} + 2D_{26}\kappa_y\kappa_{xy} + D_{66}\kappa_{xy}^2 \end{bmatrix} dxdy \tag{6}$$

where A_{ij} and D_{ij} are the in-plane and out-of-plane stifnesses, respectively. For straight fiber panels, the A_{ij} and D_{ij} may be moved out of the integral since they are independent of x and y. However, for variable-stiffness panels the A_{ij} and D_{ij} are functions of the panel coordinates and must remain as part of the integrand.

The potential energy of the external loads is given by

$$W = \lambda_1[F_x u^0{}_{(x=a)} + F_y v^0{}_{(y=b)} + p\int_0^a\int_0^b wdxdy] + \\ \lambda_2 F_x^B u^0{}_{(x=a)} \tag{7}$$

Following the Rayleigh-Ritz procedure the displacement functions are assumed of the form,

$$w(x,y) = \sum_{i=1}^{n_t} a_i \Phi_i^w$$

$$u^0(x,y) = b_0\frac{x}{a} + \sum_{i=1}^{2n_t} b_i \Phi_i^u \tag{8}$$

$$v^0(x,y) = c_0\frac{y}{b} + \sum_{i=1}^{2n_t} c_i \Phi_i^v$$

where n_t is the number of terms, a_i, b_i and c_i are the Ritz coefficients.

Depending on the choice of the functions Φ_i^w, Φ_i^u and Φ_i^v, different boundary conditions can be modelled. Since the panel edges are bounded by different structural elements like stringers, frames and other adjacent panels, the boundary conditions can be very complex. In the current work, we

assume linearly varying deformable straight edges clamped at ($x = 0$, $x = a$) and simply supported at ($y = 0$, $y = b$). The boundary conditions can be summarized as,

at $x = 0$, $u^0(0,y) = 0$, $v^0(0,y) = c_0 \dfrac{y}{b}$, $w(0,y) = 0$, and $w_{,x}(0,y) = 0$.

at $x = a$, $u^0(a,y) = b_0$, $v^0(a,y) = c_0 \dfrac{y}{b}$, $w(a,y) = 0$, and $w_{,x}(a,y) = 0$.

at $y = 0$, $v^0(x,0) = 0$, $u^0(x,0) = b_0 \dfrac{x}{a}$, and $w(x,0) = 0$

at $y = b$, $v^0(x,b) = c_0$, $u^0(x,b) = b_0 \dfrac{x}{a}$, and $w(x,b) = 0$.

where a comma (",") in subscript indicates derivative with respect to the variable following it.

For the assumed boundary conditions the displacement filed is given by

$$w(x,y) = \sum_{i=1}^{n_t} \sum_{j=1}^{n_t} a_{ij} \left(\cos \frac{(i-1)\pi x}{a} - \cos \frac{(i+1)\pi x}{a} \right) \sin \frac{j\pi y}{b}$$

$$u^0(x,y) = b_0 \frac{x}{a} + \sum_{i=1}^{2n_t} \sum_{j=1}^{2n_t} b_{ij} \sin \frac{i\pi x}{a} \sin \frac{j\pi y}{b} \qquad (9)$$

$$v^0(x,y) = c_0 \frac{y}{b} + \sum_{i=1}^{2n_t} \sum_{j=1}^{2n_t} c_{ij} \sin \frac{i\pi x}{a} \sin \frac{j\pi y}{b}$$

The number of the assumed terms for in-plane displacements u^0 and v^0 is twice that of out-of-plane displacement in w. This is done to ensure that the in-plane equilibrium is adequately satisfied.

By using the stationary conditions of total potential and minimizing with respect to Ritz coefficients a_i, b_i and c_i we obtain the general equilibrium equations for a symmetric and balanced laminated composite plate (see Appendix for details),

$$-(\lambda_1 F_x + \lambda_2 F_x^B) + K_{il}^{ub} b_i +$$
$$K_{il}^{uc} c_i + K_{ijl}^{uaa} a_i a_j = 0$$
$$-\lambda_1 F_y + K_{il}^{vb} b_i + K_{il}^{vc} c_i +$$
$$K_{ijl}^{vaa} a_i a_j = 0 \qquad (10)$$
$$K_{il} a_i + K_{ikl}^{wba} b_i a_k + K_{ikl}^{wca} c_i a_k +$$
$$K_{ijkl}^{waaa} a_i a_j a_k - \lambda_1 P_l = 0$$

The first two equations in Eq. 10 are linear in the Ritz coefficients that are corresponding to in-plane displacements, namely b_i and c_i. Thus, the

above three equations can be reduced to a single nonlinear equation by eliminating b_i and c_i from the third equation using the first two equations. Then the final set of nonlinear equations which define an equilibrium load-deflection path is solved for a_i, and by back substitution the coefficients b_i and c_i are computed. Different techniques are available for the tracing of nonlinear equilibrium paths [11]. In this paper, we use the normal flow algorithm because of its robustness and efficiency [11].

3.1 Failure Analysis

The failure load λ^f is defined as the load level at which first failure occurs. For the purpose of predicting failure, we use Tsai-Wu failure criterion. For an orthotropic lamina under plane stress conditions, this criterion is given by

$$F = F_{11}\sigma_1^2 + 2F_{12}\sigma_1\sigma_2 + F_{22}\sigma_2^2 + $$
$$F_{66}\sigma_{12}^2 + F_1\sigma_1 + F_2\sigma_2 \qquad (11)$$

where F is the failure index, σ_1, σ_2, and σ_{12} are the in-plane stresses in the principal material directions, and F_{ij} are functions expressed in terms of the strength properties as follows

$$F_{11} = \frac{1}{X_t X_c}, \qquad F_{22} = \frac{1}{Y_t Y_c}, \qquad F_{66} = \frac{1}{S^2}$$

$$F_1 = \frac{1}{X_t} - \frac{1}{X_c}, \qquad F_2 = \frac{1}{Y_t} - \frac{1}{Y_c} \qquad (12)$$

$$F_{12} = \frac{1}{2X_t^2}[1 - X_t(F_1 + F_2) - X_t^2(F_{11} + F_{22})]$$

According to Tsai-Wu criterion, a composite fails when the following condition is violated

$$F \leq 1 \qquad (13)$$

In order to apply the Tsai-Wu criterion to variable-stiffness laminates, it must be recognized that stresses will vary as a function of location over the domain. This requires that the condition in Eq. 13 must be satisfied at every point of every ply throughout the structure, that is,

$$\underset{(x,y)}{F} \leq 1 \qquad (14)$$

4 Optimization Formulation

4.1 Maximization of the Failure Load

The optimization problem can be formulated either to minimize the weight of the structure for given applied loads or maximizing the failure load for a given thickness. In this paper, the goal of the optimization problem is to determine the optimal distribution of the fiber orientation angles (or the fiber paths) over the structure for maximum failure load. Mathematically, the problem is formulated as

$$\text{maximize} \quad \lambda^f(X) \tag{15}$$

where λ^f is the objective function representing different loading cases and X is a vector of design variables.

4.2 Fiber Path Definitions and Design Variables

Varying the stiffness throughout the structure requires defining the fiber orientation variations. In the next sections linear and nonlinear variation of fiber orientation angles will be described.

4.2.1 Linear Variation of Fiber Orientation Angles

Simple forms of linear variation of fiber orientation angles for rectangular panels have been described in the literature [1]. For example,

$$\theta(x) = (T_1 - T_0)\frac{x}{a} + T_0 \tag{16}$$

where T_0 is the fiber orientation angle at $x = 0$ and T_1 is the fiber orientation angle at $x = a$. Or, alternatively,

$$\theta(x) = \frac{2(T_1 - T_0)}{a}|x| + T_0 \tag{17}$$

where T_0 is the fiber orientation angle at the panel center, $x = 0$, and T_1 is the fiber orientation angle at the panel ends, $x = \pm a/2$.

4.2.1 Nonlinear Variation of Fiber Orientation Angles

In a previous study [7] a definition of a unidirectional variation based on a nonlinear function for the fiber orientation angle was introduced. The nonlinear function was defined using Lobatto-Legendre polynomials. The definition of unidirectional variation can be generalized to be applied to spatially varying fiber orientation angles as demonstrated in this section. Assume a rectangular domain as shown in Fig. 3.
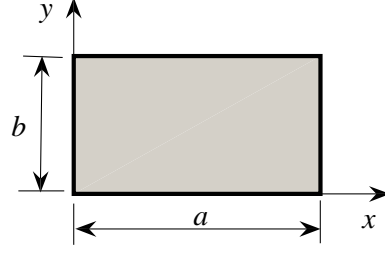
Fig. 3. Rectangular domain and coordinate system

We define the normalized coordinates ξ and η as follows

$$\xi = \frac{2x - a}{a}, \eta = \frac{2y - b}{b} \tag{18}$$

such that $-1 \le \xi \le 1, -1 \le \eta \le 1$

We define the fiber orientation angle in the $\xi - \eta$ plane by

$$\theta(\xi, \eta) = \sum_{i=0}^{m-1}\sum_{j=0}^{n-1} T_{ij}L_i(\xi)L_j(\eta) \tag{19}$$

where m and n are number of basis functions used in ξ and η directions, respectively, T_{ij} are unknown coefficients and L_i are the Lobatto polynomials defined as

$$L_i(\xi) = \int_{-1}^{\xi} P_{i-1}(\mu)d\mu, \quad i \ge 2 \tag{20}$$

where $L_0(\xi) = 1$ and $L_1(\xi) = \xi$, or in a recursive form

$$L_i(\xi) = \frac{1}{i}\left(\xi P_{i-1}(\xi) - P_{i-2}(\xi)\right), \quad i \ge 2 \tag{21}$$

where P_i are the Legendre polynomials given by

$$P_i(\xi) = [(2i-1)\xi P_{(i-1)} - (i-1)P_{(i-2)}]/i, \quad i \ge 2 \tag{22}$$

and where $P_0(\xi) = 1$ and $P_1(\xi) = \xi$.

For example, the first few Lobatto polynomials are

$$L_2(\xi) = \frac{1}{2}(\xi^2 - 1), L_3(\xi) = \frac{\xi}{2}(\xi^2 - 1),$$

$$L_4(\xi) = \frac{1}{8}(1 - 6\xi^2 + 5\xi^4), L_5(\xi) = \frac{1}{8}\xi(3 - 10\xi^2 + 7\xi^4).$$

By increasing the number of coefficients T_{ij} in Eq. 19 more freedom can be achieved to represent the fiber orientation angle variations. Consequently, there is better chance to capture the optimal fiber

angle distribution. Therefore, in this study the design variables are the unknown coefficients T_{ij}.

5 Application and Results

Results are obtained for a square ($a/b = 1$), symmetric and balanced laminate with the variable-stiffness lay-up $[\pm\theta(x, y)]_{8s}$. The number of laminate plies is $N = 16$. Each ply has a constant thickness $t = 0.254$ mm (0.01 in), i.e. the total thickness is $h = N t$. The composite material is typical graphite-epoxy with stiffness and strength properties given in Table 1 [12]. The pressure load is $p = 103.42\times10^{-3}$ MPa (15 psi) and the fuselage radius is $R = 2540$ mm (100 in). The underlying goal of the optimization problems is to determine the optimal fiber paths over the structure for maximum failure load.

Table 1. Material properties

Material properties	Graphite-Epoxy
E_1	207 GPa (30×10^6 psi)
E_2	5 GPa (0.75×10^6 psi)
ν_{12}	0.25
G_{12}	2.6 GPa (0.375×10^6 psi)
X_t	1035 MPa (150×10^3 psi)
Y_t	41 MPa (6×10^3 psi)
S	69 MPa (10×10^3 psi)
X_c	689 MPa (100×10^3 psi)
Y_c	117 MPa (17×10^3 psi)

The results presented in this paper are for a number of assumed terms $n_t = 3$ which gives adequate accuracy compared to finite element analysis. The nonlinear analysis is verified with that of commercial finite element package ABAQUS using S4R element. The loads F_x and F_y are proportional to the pressure load, as stated earlier, and the compressive load is $F_x^B = -2F_x$. The values of the stresses in the principal material directions are compared for different designs. For the upper ply of the panel ($z = h/2$), for example, the stresses at the plate center are shown in Fig. 4 as functions of the load factor. It is clear that the Rayleigh-Ritz analysis model developed agrees well with the finite element analysis. It has been found that the maximum error, in terms of stresses, is within less than 10%, which makes it adequate for preliminary design purposes.
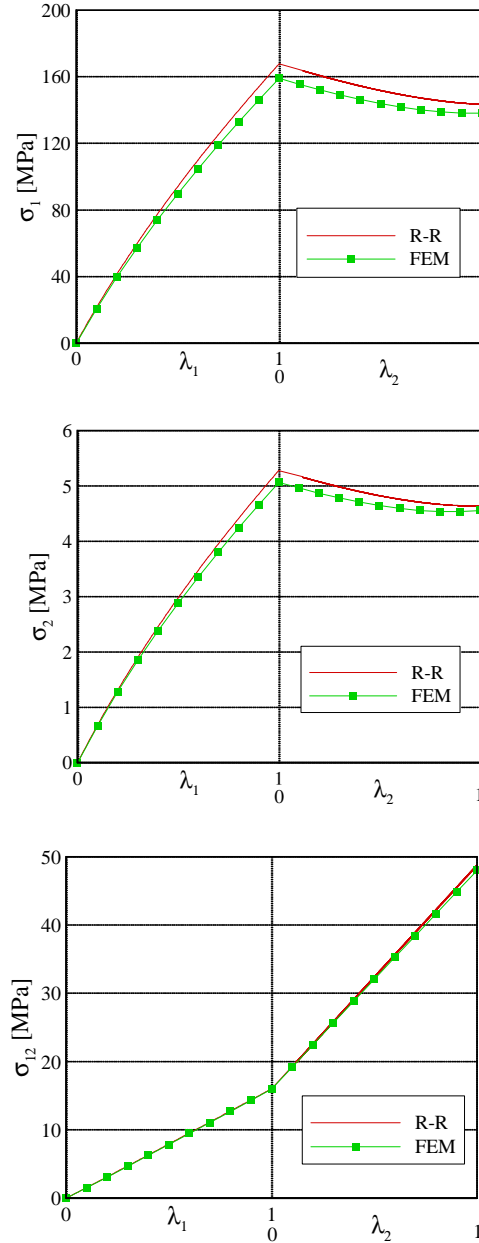
Fig. 4. Stresses in the principal material directions of the $[\pm45^0]_{8s}$ design using R-R and FEM

In this paper, as mentioned earlier, two loading cases are considered. The first loading case is a plate subjected to pressure only (no in-plane loads) which will be called Case I, and the second case is a plate subjected to a combination of pressure and in-plane tensile loads applied in the first loading step in addition to an in-plane compressive load which is applied in the second loading step. This latter case will be called Case II.

5.1 Case I: Plate Subjected to Pressure

In order to better understand the developing designs, the fiber orientation angle will initially be varied as a function of x only, $\theta = \theta(x)$, and then it will be varied spatially as a function of both x and y coordinates, $\theta = \theta(x,y)$.

5.1.1 $\theta = \theta(x)$

5.1.1.1 Linear Variation of Fiber Orientation Angles

Prior to the optimization work, we first analyze the plate using linear variation of fiber orientation angles given by Eq. 17. The pressure failure load is calculated parametrically for various combinations of the angles T_0 and T_1 in the range $0^0 \leq \theta \leq 90^0$. The results of this study are shown in Fig. 5. The thick line in the figure is for constant-stiffness straight fiber format panels. For variable-stiffness panels a family of curves corresponding to various values of T_0 and T_1 is available in Fig. 5. Each curve is generated by varying the value of T_0 between 0^0 and 90^0 for a given value of T_1 as labeled in the figure. Intersection of these curves with the curve for the straight fiber panel is a panel where T_0 is equal to T_1 value. Clearly, for constant-stiffness laminates the maximum failure load is achieved for a[$\pm 25\,^{o}$]$_{8s}$ laminate and the corresponding failure load is $\lambda_1^f = 5.56$. However, the maximum failure load that can be achieved for a variable-stiffness configuration is $\lambda_1^f = 6.19$, and is obtained for $T_0 = 0^0$ and $T_1 = 25^0$. This value is about 10% higher than the maximum value obtained with a straight fiber configuration.

It can also be observed from Fig. 5 that for a given value of T_0 the values of the failure load do not increase monotonically when the values of T_1 increase. Therefore, search for an optimal solution using traditional gradient based approaches are likely to be trapped in local optima. Accordingly, the simplex method [13] is used as the design optimization platform. Since this method uses only function value information in the search for optima, the search is repeated with different initial points to avoid getting stuck in local optima.

5.1.1.2 Nonlinear Variation of Fiber Orientation Angles

In order to verify the optimization step, we first consider the linear fiber orientation variation given by Eq. 16. The result obtained by solving the optimization problem is $T_0 = T_1 = 25^0$ with

$\lambda_1^f = 5.56$, which is the same design obtained from the analysis.

At this point, the optimization problem can be solved for different number of design variables (coefficients T_{ij}) using the more general form of fiber orientation variation given by Eq. 19 after setting the terms that include y to zero. The improvement in the load carrying capacity obtained using the steered fiber designs compared to the straight fiber design is shown in Table 2. The number of design variables is increased until the load carrying capacity improvement becomes insignificant. The optimal fiber orientation distributions for different number of design variables as well as the optimal design obtained using the linear variation are shown in Fig. 6.
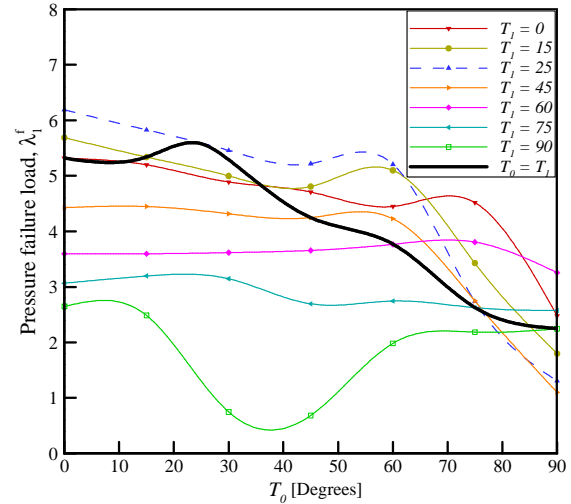
Fig. 5. Pressure failure load performance using linear variation of fiber orientation angles, (Case I)

Table 2. Load carrying capacity improvement (steered fiber vs. straight fiber), $\theta = \theta(x)$, (Case I)

Design type	No. of design variables	Failure load λ_1^f	Load carrying capacity improvement [%]
Constant-stiffness $\left[\pm 25^0\right]_{8s}$	2	5.56	-
Variable-stiffness (Linear variation)	-	6.19	10.2
Variable-stiffness	5	6.51	14.6
Variable-stiffness	8	6.87	19.0
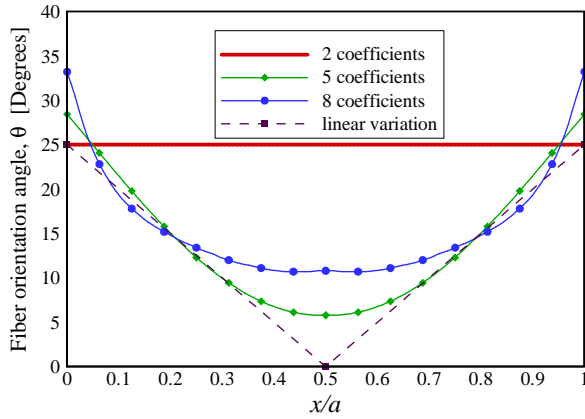
Fig. 6. Optimal distributions of the fiber orientation angles, $\theta = \theta(x)$, (Case I)
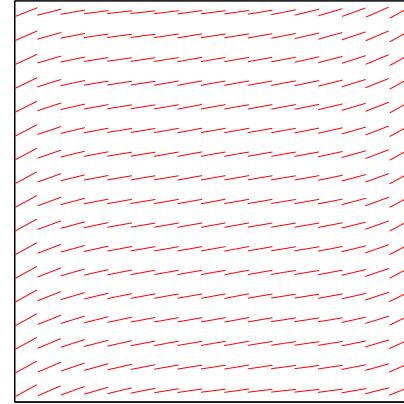
Fig. 7. Optimal distribution of the fiber orientation angles for maximum failure load (Case I)

5.1.2 $\theta = \theta(x,y)$

Varying the fiber orientation spatially as a function of x and y gives more freedom to the fibers to curve within the lamina and consequently additional improvement in the load carrying capacity may be achieved. A comparison between the constant-stiffness and the variable-stiffness designs, for different number of design variables, is shown in Table 3. The optimal distribution of the fiber orientation angles for $m = n = 6$ (36 coefficients) is depicted in Fig. 7. In order to generate the fiber paths from the fiber orientation distribution, a special code has been utilized [14]. The optimal fiber paths corresponding to the fiber orientation distribution for $m = n = 6$ are depicted in Fig 8.
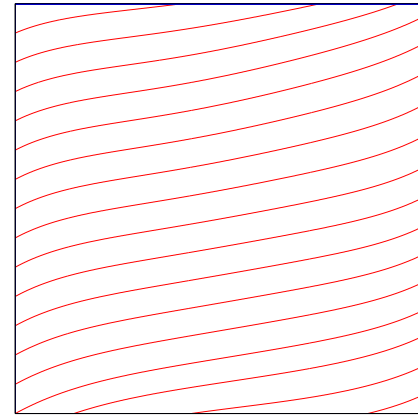
Table 3. Load carrying capacity improvement (steered fiber vs. straight fiber), $\theta = \theta(x,y)$, (Case I)

Design type	No. of design variables ($m \times n$)	Failure load λ_1^f	Load carrying capacity improvement [%]
Constant-stiffness $\left[\pm 25^0 \right]_{8s}$	-	5.56	-
Variable-stiffness	4×4	6.65	16.4
Variable-stiffness	5×5	6.95	20.0
Variable-stiffness	6×6	7.43	25.2

Fig. 8. Optimal fiber paths for maximum failure load, (Case I)

It is clear that the fiber orientation distribution that results from the use of 6×6 coefficients in the fiber angle expansion produces the maximum pressure failure load providing a load carrying capacity improvement of 25% over the optimal straight fiber design. It can also be observed that the fiber orientation variation, or in other words, the stiffness variation is higher within the bending boundary layer (in the vicinity of the clamped edges where the bending moment is large) than the stiffness variation in the center section of the panel where the stiffness is almost constant.

In order to demonstrate the values of the fiber orientation angles which are now functions of both x and y, the fiber orientations are plotted as functions of x at two different sections in the panel, $y/b = 0$ and $y/b = 0.5$. The fiber orientation distributions at those sections, along with that for 8 coefficients,

where the fiber orientation has been varied along x only, are shown in Fig. 9. It is clear that the fiber orientation distribution at $y/b = 0$ is asymmetric about $x/a = 0.5$, while it becomes symmetric at $y/b = 0.5$ showing a similar trend to the fiber orientation distribution for $\theta = \theta(x)$, with slight variations of the fiber orientation angles away from the clamped edges.
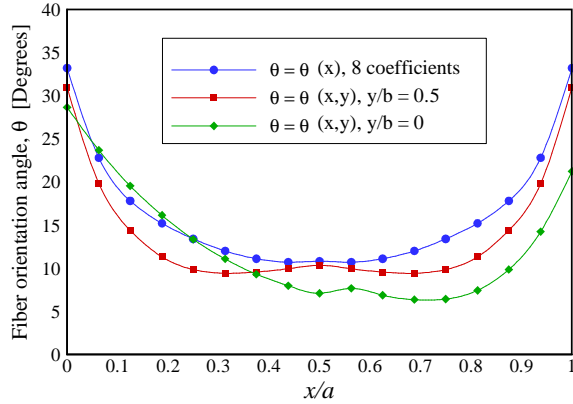
Fig. 9. Fiber orientation distributions for $\theta = \theta(x)$, and for $\theta = \theta(x,y)$ at different sections, (Case I)

5.2 Case II: Plate Subjected to Pressure, tensile and compressive loads

In the current case, It is assumed that the pressure and the pressure-induced tensile loads are constant ($\lambda_1 = 1$) in the first loading step, and the compressive load is $F_x^B = -2\,\lambda_2\,F_x$ to ensure that the panel fails in the second loading step. The goal is to maximize the in-plane compressive failure load by introducing λ_2^f as an objective function.

Similar to Case I, the optimal constant-stiffness design may be determined by considering two design variables. The optimal straight fiber design obtained is $[\pm 62^0]_{8s}$ and the corresponding compressive failure load is $\lambda_2^f = 1.911$. For variable-stiffness designs, the fiber orientation is varied spatially as a function of x and y, $\theta = \theta(x,y)$. A comparison between the constant-stiffness and the variable-stiffness designs, for different number of design variables, is shown in Table 4.

Table. 4. Load carrying capacity improvement (steered fiber vs. straight fiber), $\theta = \theta(x,y)$, (Case II)

Design type	No. of design variables ($m \times n$)	Failure load λ_2^f	Load carrying capacity improvement [%]
Constant-stiffness $\left[\pm 62^0\right]_{8s}$	-	1.911	-
Variable-stiffness	4×7	2.075	7.9
Variable-stiffness	4×9	2.257	15.3

For the variable-stiffness designs, the optimal fiber orientation distributions for the developed designs are depicted in Fig. 10 and 11. The optimal fiber paths for $m = 4$, $n = 9$ are illustrated in Fig. 12.
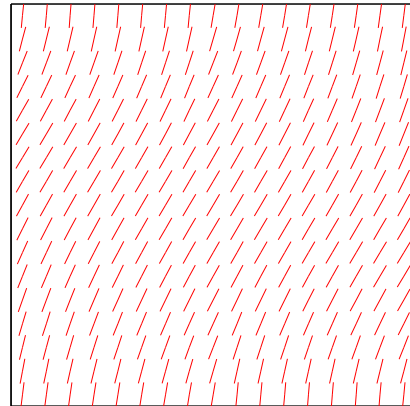
Fig. 10. Optimal distribution of the fiber orientation angles for maximum failure load, $m = 4$, $n = 7$, (Case II)
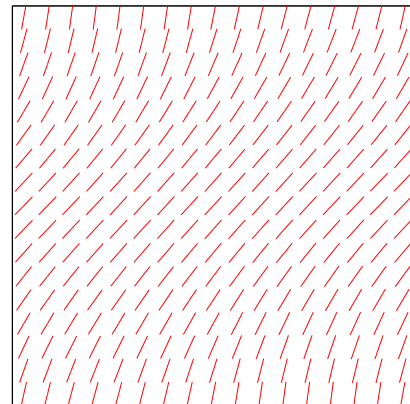
Fig. 11. Optimal distribution of the fiber orientation angles for maximum failure load, $m = 4$, $n = 9$, (Case II)
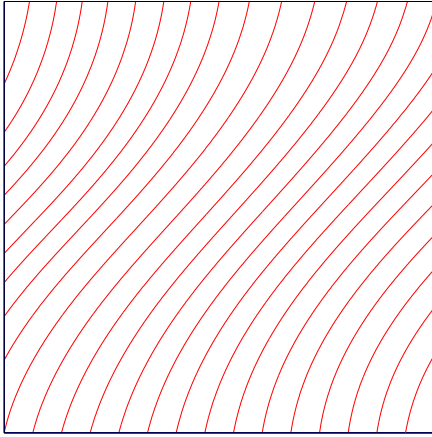
Fig. 12. Optimal fiber paths for maximum failure load,
$m = 4$, $n = 9$, (Case II)

Clearly, the maximum failure load obtained using 4×9 coefficients provides a load carrying capacity improvement of more than 15% over the optimal straight fiber design. Moreover, it can also be noticed that the fiber paths are smooth exhibiting neither discontinuities nor large curvatures. This makes the designs obtained efficient and feasible to be manufactured.

5 Conclusion

In this study, design tailoring for pressure pillowing problem of a fuselage skin panel using steered fibers was demonstrated. The optimal fiber paths over the structure were determined for maximum failure load. Optimal designs for both straight fibers and steered fibers were obtained. It was shown that by placing the fibers in their optimal spatial orientations, the pressure pillowing problem can be alleviated, and the load carrying capacity of the structure can be improved compared to traditional designs with straight fibers.

References

[1] Gürdal Z. and Olmedo R. A. "Composite laminates with spatially varying fiber orientations: Variable-stiffness panel concept". *In Proceedings of the AIAA/ASME/ASCE/AHS/ASC 33rd Structures, Structural Dynamics and Materials Conference,* Dallas, TX, volume 2, pages 798–808, 1992.

[2] Tatting B. F. and Gürdal, Z. "Enhancements of tow-steering design techniques: Design of rectangular panel under combined loads," NASA CR-2005-213911, September 2005, National Aeronautics and Space Administration, National Technical Information Service (NTIS), Springfield, VA.

[3] Jegley D., Tatting B. and Gürdal Z. "Tow- steered panels with holes subjected to compression or shear loads", *AIAA-2005-2081, 46th AIAA/ASME/AHS/ ASC Structures, Structural Dynamics and Materials Conf.,* CD-ROM, Austin, TX, 18-21 April 2005.

[4] Tatting B. F. and Gürdal Z. "Automated finite element analysis of elastically-tailored plates," NASA CR-2003-212679, December 2003, National Aeronautics and Space Administration, National Technical Information Service (NTIS), Springfield, VA.

[5] Setoodeh S., Abdalla M.M. and Gürdal Z. "Design of variable-stiffness laminates using lamination parameters". *Composites, Part B: Engineering*, Vol. 37, pp 301-309, 2006.

[6] Setoodeh S., Blom A.W., Abdalla M.M. and Gürdal Z. "Generating curvilinear fiber paths from lamination parameters distribution". *Proceedings of the 47th AIAA/ASME/ASCE/AHS/ASC Structures, Structural Dynamics and Materials (SDM) Conference*, Newport, RI, paper no. 1875, 2006.

[7] Alhajahmad A., Abdalla M. M. and Gürdal Z. "Design tailoring for pressure pillowing using tow-placed steered fibers". *SAMPE '06 Fall Technical Conference,* Dallas, Texas, 2006.

[8] Watson L.T., Sosonkina M.,Melville R.C.,Morgan A.P.and Walker H.F."Algorithm 777: HOMPACK90: A suite of Fortran 90 Codes For Globally Convergent Homotopy Algorithm", *ACM transaction on Mathematical Software*, Vol. 23, No. 4, December 1997, pp. 514-549.

[9] Reddy J. N.*" Mechanics of Laminated Composite Plates, Theory and Analysis"*. CRC Press, (1997).

[10] Chia Chuen-Yuan. "*Nonlinear analysis of plates*", McGraw-Hill, Inc. 1980.

[11] Ragon S A., Gürdal Z. and Watson L. T. "Comparison of three algorithms for tracing nonlinear equilibrium paths of structural systems", *Proceedings of the 41thAIAA/ASME/ASCE/AHS/ASC Structures, Structural Dynamics and Materials Conference*, Reston, VA, USA, Vol. 1, No. 2, 2000,pp.850-860.

[12] Jones Robert M. "*Mechanics of Composite Materials"*. Taylor & Francis, Inc., second edition, (1998).

[13] Microsoft IMSL math library, Fortran 90 subroutine "DUMPOL", Minimize a function of N variables using a direct search polytope algorithm.

[14] Blom A.W., Abdalla M.M. and Gürdal Z. "Optimization of tow-placed, tailored composite laminates". *16th international conference on composite materials,* Kyoto, Japan, 2007.

Appendix

$$K_{il}^{ub} = \int_0^a \int_0^b (A_{11}\Phi_{i,x}^u \Phi_{l,x}^u + A_{66}\Phi_{i,y}^u \Phi_{l,y}^u)\,dxdy$$

$$K_{il}^{uc} = \int_0^a \int_0^b (A_{12}\Phi_{i,y}^v \Phi_{l,x}^u + A_{66}\Phi_{i,x}^v \Phi_{l,y}^u)\,dxdy$$

$$K_{ijl}^{uaa} = \frac{1}{2}\int_0^a \int_0^b \left(A_{11}\Phi_{i,x}^w \Phi_{j,x}^w \Phi_{l,x}^u + A_{12}\Phi_{i,y}^w \Phi_{j,y}^w \Phi_{l,x}^u + A_{66}\Phi_{i,x}^w \Phi_{j,y}^w \Phi_{l,y}^u + A_{66}\Phi_{i,y}^w \Phi_{j,x}^w \Phi_{l,y}^u\right)dxdy$$

$$K_{il}^{vb} = \int_0^a \int_0^b (A_{12}\Phi_{i,x}^u \Phi_{l,y}^v + A_{66}\Phi_{i,y}^u \Phi_{l,x}^v)\,dxdy$$

$$K_{il}^{vc} = \int_0^a \int_0^b (A_{22}\Phi_{i,y}^v \Phi_{l,y}^v + A_{66}\Phi_{i,x}^v \Phi_{l,x}^v)\,dxdy$$

$$K_{ijl}^{vaa} = \frac{1}{2}\int_0^a \int_0^b \left(A_{12}\Phi_{i,x}^w \Phi_{j,x}^w \Phi_{l,y}^v + A_{22}\Phi_{i,y}^w \Phi_{j,y}^w \Phi_{l,y}^v + A_{66}\Phi_{i,x}^w \Phi_{j,y}^w \Phi_{l,x}^v + A_{66}\Phi_{i,y}^w \Phi_{j,x}^w \Phi_{l,x}^v\right)dxdy$$

$$K_{il} = \int_0^a \int_0^b \left(\begin{array}{l} D_{11}\Phi_{i,xx}^w \Phi_{l,xx}^w + \ D_{12}\Phi_{i,yy}^w \Phi_{l,xx}^w + \ D_{12}\Phi_{i,xx}^w \Phi_{l,yy}^w + \ D_{22}\Phi_{i,yy}^w \Phi_{l,yy}^w + 2D_{16}\Phi_{i,xx}^w \Phi_{l,xy}^w + \\ 2D_{16}\Phi_{i,xy}^w \Phi_{l,xx}^w + 2D_{26}\Phi_{i,yy}^w \Phi_{l,xy}^w + 2D_{26}\Phi_{i,xy}^w \Phi_{l,yy}^w + 4D_{66}\Phi_{i,xy}^w \Phi_{l,xy}^w \end{array} \right)dxdy$$

$$K_{ikl}^{wba} = \int_0^a \int_0^b \left(A_{11}\Phi_{i,x}^u \Phi_{k,x}^w \Phi_{l,x}^w + A_{12}\Phi_{i,x}^u \Phi_{k,y}^w \Phi_{l,y}^w + A_{66}\Phi_{i,y}^u \Phi_{k,y}^w \Phi_{l,x}^w + A_{66}\Phi_{i,y}^u \Phi_{k,x}^w \Phi_{l,y}^w\right)dxdy$$

$$K_{ikl}^{wca} = \int_0^a \int_0^b \left(A_{12}\Phi_{i,y}^v \Phi_{k,x}^w \Phi_{l,x}^w + A_{22}\Phi_{i,y}^v \Phi_{k,y}^w \Phi_{l,y}^w + A_{66}\Phi_{i,x}^v \Phi_{k,y}^w \Phi_{l,x}^w + A_{66}\Phi_{i,x}^v \Phi_{k,x}^w \Phi_{l,y}^w\right)dxdy$$

$$K_{ijkl}^{waaa} = \frac{1}{2}\int_0^a \int_0^b \left(\begin{array}{l} A_{11}\Phi_{i,x}^w \Phi_{j,x}^w \Phi_{k,x}^w \Phi_{l,x}^w + A_{12}\Phi_{i,y}^w \Phi_{j,y}^w \Phi_{k,x}^w \Phi_{l,x}^w + A_{12}\Phi_{i,x}^w \Phi_{j,x}^w \Phi_{k,y}^w \Phi_{l,y}^w + A_{22}\Phi_{i,y}^w \Phi_{j,y}^w \Phi_{k,y}^w \Phi_{l,y}^w + \\ A_{66}\Phi_{i,x}^w \Phi_{j,y}^w \Phi_{k,y}^w \Phi_{l,x}^w + A_{66}\Phi_{i,x}^w \Phi_{j,y}^w \Phi_{k,x}^w \Phi_{l,y}^w + A_{66}\Phi_{i,y}^w \Phi_{j,x}^w \Phi_{k,y}^w \Phi_{l,x}^w + A_{66}\Phi_{i,y}^w \Phi_{j,x}^w \Phi_{k,x}^w \Phi_{l,y}^w \end{array} \right)dxdy$$

$$\mathrm{P}_l = \int_0^a \int_0^b p\Phi_l^w\,dxdy$$